Wave propagation through penetrable scatterers in a waveguide and through a penetrable grating

Agnès Maurel[a)]
Institut Langevin, CNRS, ESPCI ParisTech, 1 rue Jussieu, 75005 Paris, France

Jean-François Mercier
Poems CNRS, ENSTA ParisTech INRIA, 828 boulevard des Maréchaux, 91762 Palaiseau, France

Simon Félix
LAUM CNRS, Université du Maine, avenue Olivier Messiaen, 72085 Le Mans, France

(Received 21 June 2013; revised 15 October 2013; accepted 12 November 2013)

A multimodal method based on the admittance matrix is used to analyze wave propagation through scatterers of arbitrary shape. Two cases are considered: a waveguide containing scatterers, and the scattering of a plane wave at oblique incidence to an infinite periodic row of scatterers. In both cases, the problem reduces to a system of two sets of first-order differential equations for the modal components of the wavefield, similar to the system obtained in the rigorous coupled wave analysis. The system can be solved numerically using the admittance matrix, which leads to a stable numerical method, the basic properties of which are discussed (convergence, reciprocity, energy conservation). Alternatively, the admittance matrix can be used to get analytical results in the weak scattering approximation. This is done using the plane wave approximation, leading to a generalized version of the Webster equation and using a perturbative method to analyze the Wood anomalies and Fano resonances. © *2014 Acoustical Society of America.*
[http://dx.doi.org/10.1121/1.4836075]

PACS number(s): 43.38.Hz, 43.20.Mv, 43.20.Bi [ANN] Pages: 165–174

I. INTRODUCTION

The interaction of an acoustic wave with scatterers made of penetrable material can be understood by solving the equation for the acoustic pressure p in an inhomogeneous medium,

$$\nabla \cdot \left(\frac{1}{\rho(\mathbf{r})} \nabla p(\mathbf{r}) \right) + \frac{\omega^2}{B(\mathbf{r})} p(\mathbf{r}) = 0, \tag{1}$$

with ω the angular frequency. Here, the mass density ρ and bulk modulus B can vary with position $\mathbf{r}$, allowing contrasts between the host medium and the scatterers. Equation (1) can be used for electromagnetic waves and for water waves in shallow water area. In this paper, we are interested in two families of geometrical configurations: (A) guided waves interacting with scatterers contained in a rigid waveguide; and (B) scattering by a periodic row of scatterers. Case (A) includes the possibility of various sources, such as point sources or incident beams, and arbitrary distribution and shapes of scatterers, as used in many applications (see, e.g., the application to blood cell characterization,[1] acoustic non-destructive testing in complex guiding structures[2] or passive optical components in optical waveguides[3]). In the case of an incident plane wave and a centered scatterer, the configuration becomes equivalent to an incident plane wave impinging on an infinite periodic row of scatterers with normal incidence, because the Neumann boundaries create an infinite number of images. This leads naturally to configuration (B) where we generalize to a wave at oblique incidence to an array of scatterers located periodically (gratings). This configuration has been extensively studied in the context of electromagnetism because of the increasing interest in the properties of photonic crystals and subwavelength gratings. Inspired by the observations in electromagnetism, the concepts have been transposed to acoustics,[4,5] water waves,[6] and elasticity.[7–9]

We propose a multimodal method based on the use of the admittance matrix to solve these problems. Our motivation is twofold: on the one hand, multimodal methods are efficient when compared to other numerical methods (reviews can be found in Refs. 10 and 11), on the other hand, they offer a nice tool to inspect limiting cases where simple analytical results are possible. In its numerical implementation, our method is directly inspired from the works initiated in the context of acoustic waveguides with varying cross section[12] for application to musical instruments[13–15] and later extended to more complex geometries[16,17] and to elastic waves.[18] The wave equation is first projected onto the modal basis, which reduces the problem to a set of coupled differential equations for the modal components of the fields. Solving the differential system is done by introducing the admittance matrix, which allows us to get an efficient and stable numerical method. Indeed, it gives a boundary value problem which can be integrated starting from the radiation condition, and it avoids the problems of the numerical contamination of the solution due to the exponential growth of evanescent modes.[12,19,20] For gratings in electromagnetism, the most popular multimodal method is the rigorous coupled

[a)]Author to whom correspondence should be addressed. Electronic mail: agnes.maurel@espci.fr

wave analysis (RCWA), combined with S-matrix or R-matrix algorithms.[19,21–23] Our approach differ by mainly two points: (i) by means of the weak formulation of Eq. (1), the resulting coupled mode equations naturally account for the right continuity conditions at the scatterer interface, increasing the accuracy compared with the common staircase approximation (cf. Sec. III C); (ii) the admittance matrix, Y, is used instead of the S- or R-matrix. It is a local operator, governed by a differential Riccati equation, and this makes Y, by construction, well suited to deal with continuously varying media. Also, the Riccati equation can be solved analytically in limiting cases, and this is exemplified in the paper.

The method is presented in Sec. II. The properties of reciprocity and energy conservation are shown and tested including at the cutoff frequencies (Sec. III B). Modal expansions may offer physical insights of the wave phenomena since the modes used are exact solutions of the trivial problem, that is, the problem without scatterer.[24] In Sec. IV, three simple analytical results are derived and compared to direct numerical calculations. In the low frequency regime, the Webster equation describes the propagation of a wave in a waveguide with varying cross section.[25,26] A generalization of the Webster equation is obtained and it is used for two particular shapes of scatterers. Also, the reflection by a grating made of a penetrable material is considered. Following the work of Hessel and Oliner,[27] we analyze the Wood anomalies, appearing at and near the cutoff frequencies. This provides approximate expressions for the reflection coefficients at each interference order. The Fano resonances, corresponding to the existence of two close anomalies, are shown to exist for a contrast in B only.

II. DERIVATION AND NUMERICAL INTEGRATION OF THE MULTIMODAL FORMULATION

In this section, the problem of the scattering by penetrable scatterers is treated using a weak formulation, Eq. (7), that exactly accounts for the boundary conditions at the scatterer boundaries, Eq. (3). Expanding the solution onto a basis of transverse functions leads to a system of coupled wave equations governing the multimodal wavefield, Eq. (10). This system applies to the case of scatterers in waveguides with hard walls and to the case of a grating of scatterers, depending on the choice of the transverse functions, Eq. (6). Then, the numerical scheme is presented. It is based on the use of the so-called admittance matrix, which translates the Dirichlet to Neumann operator for the modal components.

A. Formulation

The wavefield $p(\mathbf{r})$ satisfies the wave equation (1) in the 2D-space $\mathbf{r} = (x, y)$ (the time dependence $e^{-i\omega t}$ will be omitted in the following). The scatterers present a contrast in both the mass density and the bulk modulus, and we note (ρ_0, B_0) the quantities inside the scatterers and (ρ, B) in the host medium, ρ_0, B_0, ρ, and B being constant. The scatterers are located within a region $0 \le x \le L$ and they have arbitrary shapes. Introducing Ω_0 and Ω_{ext}, respectively the space occupied by the penetrable scatterers and the part of the waveguide outside the scatterers, p_0 and p the solutions in Ω_0 and Ω_{ext}, Eq. (1) may also be written

$$\begin{cases} \left(\Delta + \dfrac{\rho_0\omega^2}{B_0}\right)p_0 = 0 & \text{in } \Omega_0, \\ \left(\Delta + \dfrac{\rho\omega^2}{B}\right)p = 0 & \text{in } \Omega_{\text{ext}}, \end{cases} \tag{2}$$

with the following (essential and natural) boundary conditions at the scatterers boundary

$$p_0 = p \quad \text{and} \quad \frac{1}{\rho_0}\frac{\partial p_0}{\partial n} = \frac{1}{\rho}\frac{\partial p}{\partial n}, \tag{3}$$

where $\mathbf{n}$ is the exterior normal of the scatterers. The forcing is an incident field $p^{(\text{inc})}$ satisfying the wave equation in the absence of scatterer. Finally p satisfies radiation conditions at $x = 0$ and L, where the scattered pressure field corresponds to outgoing waves.

Two configurations are considered, as illustrated in Fig. 1. In the first configuration (A), scatterers are contained in a waveguide of height h with Neumann boundary conditions at $y = 0$, h. In the second configuration (B), an infinite periodic row of scatterers is considered with a h-periodicity along the y axis on which an incident plane wave $p^{(\text{inc})} = e^{i(\alpha x + \beta y)}$ is sent. This latter case can be solved by considering a single scatterer with periodic boundary conditions, the essential condition $p(x, h) = p(x, 0)e^{i\beta h}$ and the natural condition $\partial_y p(x, h) = \partial_y p(x, 0)e^{i\beta h}$, β being the vertical component of the wave vector, constant for the whole problem.

The wavefield $p(x, y)$ is now developed as

$$p(x, y) = \sum_m p_m(x)\varphi_m(y), \tag{4}$$

with $\{\varphi_m\}$ a basis of transverse functions satisfying the orthogonality relations

$$(\varphi_n,\, \varphi_m) = \delta_{mn} \quad \text{and} \quad (\varphi'_n,\, \varphi'_m) = \gamma_n^2\delta_{mn}, \tag{5}$$

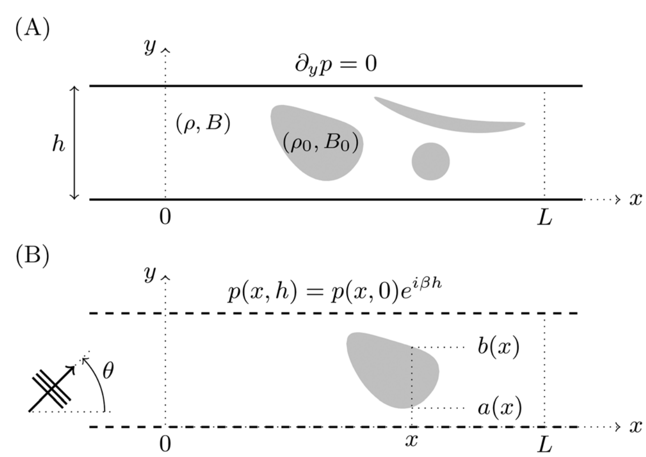

FIG. 1. Two configurations are studied. (A) The scatterers are contained in a 2D waveguide with Neumann boundary conditions at the walls. (B) An infinite periodic row of scatterers is considered.

with $(f,g)=\int_0^h \mathrm{d}y\, f\bar{g}$ the scalar product. These functions are chosen to satisfy the same boundary conditions as the wavefield p, namely,

$$\text{(A)},\ \varphi_n(y)\equiv\sqrt{\frac{2-\delta_{n0}}{h}}\cos\left(n\pi\frac{y}{h}\right),\qquad n\in\mathbb{N},$$
$$\text{(B)},\ \varphi_n(y)\equiv\frac{1}{\sqrt{h}}e^{i(\beta+2n\pi/h)y},\qquad n\in\mathbb{Z}.\tag{6}$$

Following Ref. 24, the wave equation (1) is written in a weak formulation, also called weighted residuals method

$$\int_\Omega \mathrm{d}\mathbf{r}\ [\nabla p\cdot\nabla\bar{q}-k^2p\bar{q}] + \int_{\Omega_0}\mathrm{d}\mathbf{r}\left[\left(\frac{\rho}{\rho_0}-1\right)\nabla p\cdot\nabla\bar{q}-k^2\left(\frac{B}{B_0}-1\right)p\bar{q}\right]=0,\tag{7}$$

where $k^2\equiv\omega^2\rho/B$ and where $q(\mathbf{r})=Q(x)\varphi_n(y)$ is a test function compactly supported, $\Omega=\Omega_0\cup\Omega_{\mathrm{ext}}$ denotes the whole space of the waveguide. Note that for N scatterers (see Fig. 1) occupying domains Ω_i, $i=1,\ldots,N$, the integral over $\Omega_0=\cup_{i=1,\ldots,N}\Omega_i$ has to be understood as the sum of integrals over Ω_i, $i=1,\ldots,N$.

Integrating Eq. (7) over y, the equation ends with $\int \mathrm{d}xQ(x)f(x)=0$ for any Q, from which $f(x)=0$ is deduced. This leads to

$$\partial_x\left[p'_n+\left(\frac{\rho}{\rho_0}-1\right)\mathsf{C}_{nm}p'_m\right]+k_n^2p_n - \left(\frac{\rho}{\rho_0}-1\right)\mathsf{D}_{nm}p_m+k^2\left(\frac{B}{B_0}-1\right)\mathsf{C}_{nm}p_m=0,\tag{8}$$

where we used the Einstein summation convention and where

$$\begin{cases}\mathsf{C}_{nm}(x)\equiv\displaystyle\int_{a(x)}^{b(x)}\mathrm{d}y\ \varphi_n(y)\ \overline{\varphi_m(y)},\\ \mathsf{D}_{nm}(x)\equiv\displaystyle\int_{a(x)}^{b(x)}\mathrm{d}y\ \varphi'_n(y)\ \overline{\varphi'_m(y)},\end{cases}\tag{9}$$

and $[a(x),b(x)]$ are a parameterization of the interface between one scatterer and the host medium (Fig. 1). For all x values, a scatterer occupies $y\in[a(x),\ b(x)]$, and $a=b$ is imposed when there is no scatterer at the x position. In the case where the cross section at x intersects more than one scatterer, the result follows by linearity: C_{nm} and D_{nm} are the sums of the integrals (9) over the segments $[a_i(x),\ b_i(x)]$ of the ith scatterer.

Defining the quantity $q_n\equiv p'_n+(\rho/\rho_0-1)\mathsf{C}_{nm}p'_m$, the above equation can be written as a set of first-order coupled equations governing the modal components $\mathbf{p}\equiv(p_m)$ and $\mathbf{q}\equiv(q_m)$,

$$\begin{pmatrix}\mathbf{p}\\ \mathbf{q}\end{pmatrix}'=\begin{pmatrix}0 & \mathsf{E}^{-1}\\ \mathsf{K}^2+\mathsf{F} & 0\end{pmatrix}\begin{pmatrix}\mathbf{p}\\ \mathbf{q}\end{pmatrix}\tag{10}$$

where K is a diagonal matrix with $K_n=ik_n$, $k_n^2\equiv k^2-\gamma_n^2$. Matrices E and F are defined by

$$\mathsf{E}(x)\equiv\mathsf{I}+(\rho/\rho_0-1)\,\mathsf{C}(x),$$
$$\mathsf{F}(x)\equiv(\rho/\rho_0-1)\,\mathsf{D}(x)-k^2(B/B_0-1)\,\mathsf{C}(x).\tag{11}$$

The above system can be written as a second-order equation on $\mathbf{p}$,

$$(\mathsf{E}\mathbf{p}')'=(\mathsf{K}^2+\mathsf{F})\mathbf{p},\tag{12}$$

in agreement with Ref. 24 In the case (B), where the projection is identical to a Fourier transform, the first equation of the above system (10) corresponds to $q_n=[\rho^{-1}]_{n-m}p_m$, with $[\rho^{-1}]_{n-m}\equiv\int \mathrm{d}y\,\rho^{-1}(\mathbf{r})\,e^{2i\pi(n-m)/h}$ (often called the Toeplitz matrix). This form is in agreement with the form derived by Li.[22] However, in Ref. 22 the form $\rho q=\partial_x p$ is first projected to get $p'_n=[\rho]_{n-m}q_m$. In this reference, within the staircase approximation (locally ρ depends on y only), the rule of Fourier factorization derived by Li, called inverse rule, states that the correct truncation of $p'_m=[\rho]_{n-m}q_m$ precisely leads to $q_n=[\rho^{-1}]_{n-m}p_m$. Ironically, our variational representation leads to the same conclusion for this equation, although no consideration on the truncation has been done. This will be discussed further in the following Sec. III B.

B. Numerical integration

There are two difficulties to solve Eq. (10). First, the contamination by exponentially growing evanescent modes has to be avoided (see, e.g., Refs. 12, 19, and 20). Second, the original problem is posed as a boundary value problem, with a forcing source at $x=0$ and a radiation condition at $x=L$. Therefore, the coupled first-order equations (10) cannot be solved directly as an initial value problem.[12] To circumvent these problems, we implement a multimodal admittance method which leads to a stable initial value problem. This method has been presented in earlier works for waveguides with varying cross section for acoustic waves[12,28] and elastic waves,[29] or for waveguides with curvature effect.[16,17] The main steps are recalled in the following.

The first step is to define the admittance matrix, which links the vector $\mathbf{q}$ to $\mathbf{p}$: $\mathbf{q}=\mathsf{Y}\mathbf{p}$. Using Eq. (10) the admittance matrix satisfies a Riccati equation,

$$\mathsf{Y}'=-\mathsf{Y}\mathsf{E}^{-1}\mathsf{Y}+\mathsf{K}^2+\mathsf{F},\tag{13}$$

that can be solved numerically from the output ($x=L$) to the input ($x=0$) of the region of interest, given an initial condition $\mathsf{Y}(L)$. Since the region $x>L$ is such that only right-going waves can propagate (the medium is uniform and contains no source), then $\mathsf{E}(x>L)=\mathsf{I}$, $\mathsf{F}(x>L)=0$ and, from Eq. (10), $\mathbf{p}'=\mathbf{q}$ and $\mathbf{q}'=\mathsf{K}^2\mathbf{p}$. It follows that

$$\mathsf{Y}(L)=\mathsf{K}.$$

Once the admittance matrix has been calculated along the x axis, the modal wavefield $\mathbf{p}$ is calculated as the solution of the first-order, numerically stable, equation

$$\mathbf{p}' = \mathsf{E}^{-1}\mathsf{Y}\mathbf{p}, \tag{14}$$

given an initial condition $\mathbf{p}(0)$.

Note that, from the calculation of Y, and without the need to compute the wavefield in a particular configuration, the scattering properties of the region of interest $\{(x,y) \in [0,L] \times [0,h]\}$ can be deduced. Indeed, the reflection matrix R, defined by $\mathbf{p}^{(\mathrm{r})}(0) = \mathsf{R}\mathbf{p}^{(\mathrm{inc})}(0)$, with $\mathbf{p}^{(\mathrm{inc})}$ the incident wave and $\mathbf{p}^{(\mathrm{r})}$ the reflected wave, can be written as

$$\mathsf{R} = [\mathsf{K} + \mathsf{Y}(0)]^{-1}[\mathsf{K} - \mathsf{Y}(0)]. \tag{15}$$

The transmission matrix T, defined by $\mathbf{p}^{(\mathrm{t})}(L) = \mathsf{T}\mathbf{p}^{(\mathrm{inc})}(L)$, $\mathbf{p}^{(\mathrm{t})}$ being the transmitted wave, can also be calculated as following. Together with the computation of Y, one computes the propagator G, defined such that, for $x \leq L$, $\mathbf{p}(L) = \mathsf{G}(L,x)\mathbf{p}(x)$, and solution of the equation $\mathsf{G}' = -\mathsf{G}\mathsf{E}^{-1}\mathsf{Y}$ with $\mathsf{G}(L,L) = \mathsf{I}$. Then,

$$\mathsf{T} = \mathsf{G}(L,\, 0)(\mathsf{I} + \mathsf{R}). \tag{16}$$

Note that the calculation of both R and T does not require any storage of Y or G along the axis.

Following the above cited papers (see, notably, Refs. 28 and 29), one uses a Magnus scheme to solve Y, G, and $\mathbf{p}$. From Eq. (10), one writes

$$\begin{pmatrix} \mathbf{p}(x-\delta x) \\ \mathbf{q}(x-\delta x) \end{pmatrix} = e^{-\mathsf{M}\delta x} \begin{pmatrix} \mathbf{p}(x) \\ \mathbf{q}(x) \end{pmatrix} \tag{17}$$

where

$$\mathsf{M} \equiv \begin{pmatrix} 0 & \mathsf{E}^{-1} \\ \mathsf{K}^2 + \mathsf{F} & 0 \end{pmatrix}, \tag{18}$$

evaluated at $(x - \delta x/2)$. Then, writing the exponential propagator as

$$e^{-\mathsf{M}\delta x} = \begin{pmatrix} \mathsf{E}_1 & \mathsf{E}_2 \\ \mathsf{E}_3 & \mathsf{E}_4 \end{pmatrix} \tag{19}$$

an iterative scheme to compute Y, G, and $\mathbf{p}$ can be written as

$$\mathsf{Y}(x-\delta x) = [\mathsf{E}_3 + \mathsf{E}_4\mathsf{Y}(x)][\mathsf{E}_1 + \mathsf{E}_2\mathsf{Y}(x)]^{-1}, \tag{20}$$

$$\mathsf{G}(x-\delta x) = \mathsf{G}(x)[\mathsf{E}_1 + \mathsf{E}_2\mathsf{Y}(x)]^{-1}, \tag{21}$$

$$\mathbf{p}(x) = [\mathsf{E}_1 + \mathsf{E}_2\mathsf{Y}(x)]^{-1}\mathbf{p}(x-\delta x). \tag{22}$$

Note that, in a region with constant properties ρ and B, exact algebraic solutions for Y, R, T, and $\mathbf{p}$ can be written. Then, the numerical, iterative, integration of Eq. (10) is only needed in the region closely surrounding the inhomogeneity ($x \in [x_{\min}, x_{\max}]$, Fig. 2), resulting in a fast computation.

Figure 2 shows an example of computation of the wavefield generated by a point source in a waveguide containing a scatterer of any shape. The shape of the scatterer is parameterized and the point source is at $(x_s,\, y_s) = (h,\, 0.4h)$. At the chosen high frequency $kh = 19.5\pi$, 20 modes are propagating and a converged field is obtained with $N = 30$. Given two points $x_{\min}$ and $x_{\max}$, at the left and right of the scattering region and close to it, one uses iterative schemes (20)–(21), with the radiation condition $\mathsf{Y}(x_{\max}) = \mathsf{K}$, to get R, T, and the admittance matrix Y. Then the wavefield upstream from the scatterer can be written as the sum of the incident field $\mathbf{p}^{(\mathrm{inc})} = \mathbf{g}$, that is, the classical Green's function in a 2D uniform waveguide [Fig. 2(a)],

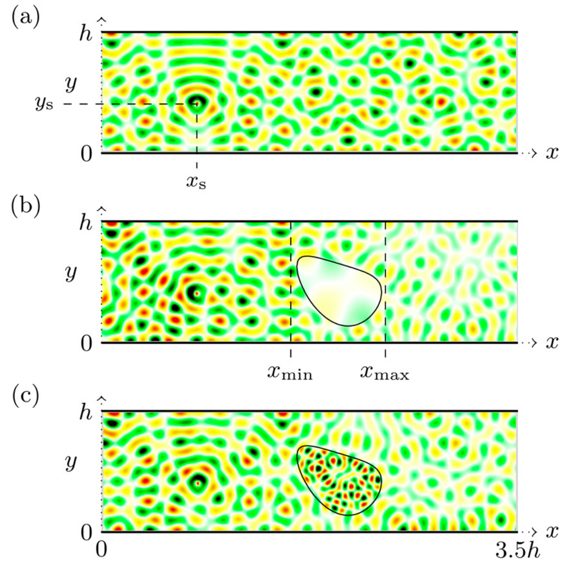

FIG. 2. (Color online) Wavefield (real part) generated by a point source in a waveguide containing a scatterer with a contrast in ρ (no contrast in B). (a) Incident wave in the empty waveguide produced by a point source, Eq. (23), with $x_s = h$, $y_s = 0.4h$. In the presence of a scatterer with contrasts (b) $\rho/\rho_0 = 10$; (c) $\rho/\rho_0 = 0.3$. $kh = 19.5\pi$, calculations have been done using $N = 30$ modes (20 propagating modes).

$$g_n(x) = \frac{\varphi_n(y_s)}{2ik_n} e^{ik_n|x-x_s|}, \tag{23}$$

and the reflected field $\mathsf{R}\mathbf{g}$. From the initial condition $\mathbf{p}(x_{\min}) = (\mathsf{I} + \mathsf{R})\,\mathbf{g}(x_{\min})$, Eq. (22) is integrated to get the wavefield in the scattering region, and the wavefield downstream from this region is simply given by $\mathsf{T}_{\mathbf{g}}$.

Two different contrasts in the mass density are considered: $\rho/\rho_0 = 10$ [Fig. 2(b)] and $\rho/\rho_0 = 0.3$ [Fig. 2(c)], while $B/B_0 = 1$ in both cases. Obviously, the wavelength change in the scattering media ($\lambda = 2\pi/k$ varies as $\lambda = \lambda_0\sqrt{\rho B_0/\rho_0 B}$) is visible.

Another example is given in Fig. 3, calculated at a higher frequency ($\lambda/h \simeq 0.03$, 71 modes are propagating) for a contrast in B only. The incident wave is obtained by weighting the modal components in Eq. (23) by a Gaussian function, as described in Ref. 30 resulting in a cluster of modes, of which one sees the ray-like behavior, and the reflection and refraction of the beam by the scatterer.

III. PROPERTIES OF THE NUMERICAL SCHEME

In this section we discuss the properties of the numerical scheme obtained from the coupled mode evolution equation, Eq. (10). First, the reciprocity and energy conservation are inspected: these properties are satisfied by the initial problem

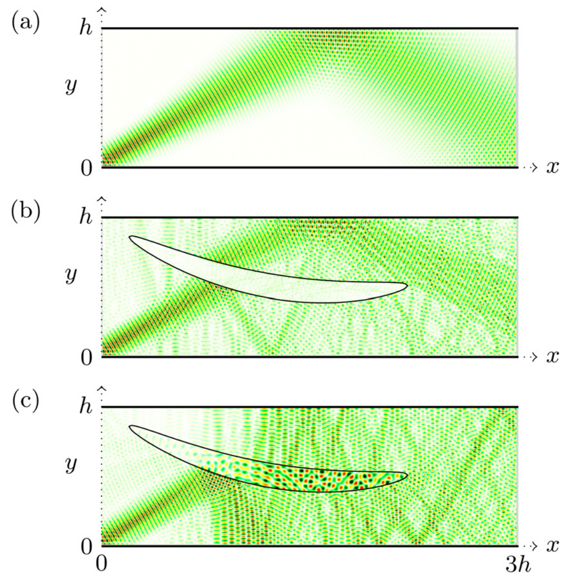

FIG. 3. (Color online) Wavefield (real part) generated by a cluster of modes in a waveguide containing a scatterer with a contrast in B (no contrast in ρ). (a) Incident beam wave; in the presence of a scatterer with contrasts (b) $B/B_0 = 10$; (c) $B/B_0 = 0.3$ for $kh = 70.5\pi$, $N = 100$ modes are taken into account in the calculations.

and it is important to check that the numerical scheme preserves them. Then, the convergence of the scattering coefficients and of the pressure field in the scattering region are presented. Finally, a discussion on the accuracy of our projection with respect to the shape of the scatterer is proposed. This is done by comparing it to the projections used in the coupled wave analysis (RCWA) and discussed in a series of papers.[22,23,31]

A. Reciprocity and energy conservation

Reciprocity links two solutions p_A and p_B of the problem, namely,

$$\nabla \cdot \left[p_A \frac{1}{\rho} \nabla p_B - \; p_B \frac{1}{\rho} \nabla p_A \right] = 0, \tag{24}$$

which translates, on our modal components, to

$$\partial_x [{}^t\mathbf{p}_A \mathbf{q}_B - {}^t\mathbf{p}_B \mathbf{q}_A)] = 0. \tag{25}$$

The energy conservation is obtained following the same procedure, choosing $p_A = p$, $p_B = \bar{p}$ which gives the conservation of the Poynting vector $\partial_x \Pi = 0$, with

$$\Pi(x) \propto \mathrm{Im}[(\rho^{-1} \partial_x p, p)] = \mathrm{Im}[({}^t\bar{\mathbf{p}}, \, \mathbf{q})]. \tag{26}$$

Since E and F are self-adjoint matrices, it follows directly that the reciprocity Eq. (25) and the energy conservation $\partial_x \Pi = 0$ are satisfied. This shows that the coupled mode equations (10) are, by construction, conservative.

To verify the reciprocity and the energy conservation of the numerical solution of Eq. (10), the following properties of the scattering matrix S are inspected:

$$\mathsf{JS} - {}^t\mathsf{SJ} = 0, \tag{27}$$

$$\mathsf{H_m} + {}^t\overline{\mathsf{S}}\mathsf{H_p} - {}^t\overline{\mathsf{S}}\mathsf{H_p}\mathsf{S} - \mathsf{H_p}\mathsf{S} = 0, \tag{28}$$

where $\mathsf{H_p} \equiv \mathsf{J} + {}^t\overline{\mathsf{J}}$, $\mathsf{H_m} \equiv \mathsf{J} - {}^t\overline{\mathsf{J}}$, and

$$\mathsf{J} \equiv \begin{pmatrix} \mathsf{K} & 0 \\ 0 & \mathsf{K} \end{pmatrix} \tag{29}$$

and these properties are expressed including the evanescent modes.[32] The first equation refers to the reciprocity and it has the same form with or without the evanescent modes. The second equation refers to the conservation of energy. In this expression, the terms involving $\mathsf{H_p}$ represent the energy flux carried out by the evanescent modes (if evanescent modes were not accounted for, we would have $\mathsf{H_p} = 0$). Finally, as already noted in Ref. 32, as soon as reciprocity and energy conservation are verified, the time-reversal invariance is also verified.

In order to test the properties (27)–(28), calculations have been performed in the case of a square scatterer centered at $y = h/2$ in a waveguide. The mode zero is sent (incident plane wave). The frequency range is chosen such that one passes through, and on, the cutting points $k_n = \sqrt{k^2 - \gamma_n^2} = 0 \, (n = 2, 4)$. These "cutoff" frequencies, associated to Wood's anomalies, are known as a delicate problem in numerical computing[4,33] (see also Sec. IV B).

We have reported in Fig. 4 the relative errors

$$\epsilon_1 = \frac{\|\mathsf{JS} - {}^t\mathsf{SJ}\|}{\|\mathsf{JS}\|}, \quad \epsilon_2 = \frac{\|\mathsf{H_m} + {}^t\overline{\mathsf{S}}\mathsf{H_p} - {}^t\overline{\mathsf{S}}\mathsf{H_p}\mathsf{S} - \mathsf{H_p}\mathsf{S}\|}{\|\mathsf{H_m} + {}^t\overline{\mathsf{S}}\mathsf{H_p}\|}, \tag{30}$$

that measure the deviation to the reciprocity property, Eq. (27), and the deviation to the energy conservation, Eq. (28). In Eq. (30), $\|M\| = \sqrt{\sum_{i,j} |M_{ij}|^2}$ In the presented cases, ϵ_1. and ϵ_2 remain within the computer precision over the whole frequency range, though a noticeable variation is observed at the cutoff frequencies.

B. Convergence

To characterize the convergence of these three formulations, the reflection coefficient $\mathsf{R}_{00}^{(N)}$ of the incident plane

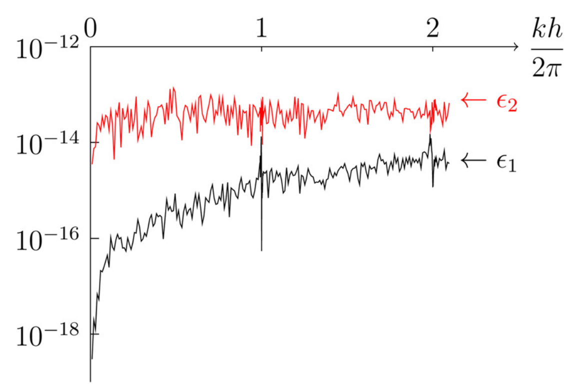

FIG. 4. (Color online) Evaluation of the properties of reciprocity and energy conservation: relative errors ϵ_1 and ϵ_2 [Eq. (30)], computed with 17 modes, as function of the nondimensional frequency $kh/2\pi$. Calculations have been performed for square scatterers of side $a = h/10$, centered at $y = h/2$, with $B/B_0 = 2$, $\rho/\rho_0 = 1$ for an incident plane wave.

wave (the central term of the reflection matrix) is computed with N modes taken into account, and compared with $\mathsf{R}^{(ex)}$, obtained with numerical simulations based on finite element methods.[34] First, the following rates of convergence are obtained

$$|\mathsf{R}_{00}^{(N)} - \mathsf{R}^{(ex)}| \propto \begin{cases} N^{-3} & \text{for a contrast in } B \text{ only,} \\ N^{-1} & \text{for a contrast in } \rho. \end{cases} \qquad (31)$$

As expected, the convergence when no contrast in ρ is considered is better, due to a higher regularity of the pressure field in that case. However, the convergence of the pressure field may differ from the convergence of the reflection coefficient. Indeed, the convergence of the reflection coefficient is given by the convergence of the propagating modes. In the scattering region, the convergence of the pressure field is limited by the convergences of both the propagating and evanescent modes. This latter convergence can be evaluated theoretically since it corresponds to the usual remainder series: it is $N^{-3/2}$ for a contrast in ρ (p is continuous but ∇p is not), and $N^{-5/2}$ for a contrast in B only (p and ∇p are continuous).

We have checked (results are not reported) that the pressure field has a convergence N^{-1} for a contrast in ρ and $N^{-5/2}$ for a contrast in B only, corresponding to the lowest convergence of both the propagating and evanescent modes. Similar low convergence of the pressure field has already been observed in the case of waveguides with varying cross section, corresponding to sound hard scatterers.[35]

C. Remark on the coupled wave analysis method

In the case of the grating (B), the convergence of multimodal method has been inspected in details in a series of papers, following the improvements proposed by Li.[22,23,31] In these references, the initial system to solve is

$$\begin{aligned} p'_n &= [\rho]_{n-m} q_m, \\ q'_n &= \gamma_n \gamma_m [\rho^{-1}]_{n-m} p_m - \omega^2 [B^{-1}]_{n-m} p_m, \end{aligned} \qquad (32)$$

where the contrast in B, which is disregarded in those references, has been added. Li shows that the convergence can be improved using the rules of Fourier factorization for truncated series. For the staircase approximation (ρ and B depend on y only), this leads to

$$\begin{aligned} p'_n &= [\rho^{-1}]^{-1}_{n-m} q_m, \\ q'_n &= \gamma_n \gamma_m [\rho]^{-1}_{n-m} p_m - \omega^2 [B^{-1}]_{n-m} p_m. \end{aligned} \qquad (33)$$

For our weak formulation taking naturally into account the boundary conditions at the scatterers interfaces, the system (10) can be written

$$\begin{aligned} p'_n &= [\rho^{-1}]^{-1}_{n-m} q_m, \\ q'_n &= \gamma_n \gamma_m [\rho^{-1}]_{n-m} p_m - \omega^2 [B^{-1}]_{n-m} p_m, \end{aligned} \qquad (34)$$

which differs slightly from Eq. (33).

To get further information on the accuracy of the three formulations, we have performed calculations for three geometries: (a) a square with sides along the x and y directions, (b) the same square with its diagonals along x and y directions, and (c) a circle. The errors $|\mathsf{R}_{00}^{(N)} - \mathsf{R}^{(ex)}|$ are reported in Fig. 5. Obviously, only the first geometry corresponds to a lamellar profile. Also two materials have been considered: (i) a nonmagnetic material ($B = B_0$) with $\rho/\rho_0 = 0.01$ and (ii) a nearly sound hard material with $B/B_0 = 6 \times 10^{-7}$ and $\rho/\rho_0 = 10^{-4}$ (corresponding to steel in air).

For the cases (ii) with high contrast in ρ, the formulation (32) does not converge. This is not surprising since it was, in fact, the observation that Eq. (32) is inaccurate to deal with metallic grating that motivated Li's works. The convergence of the Li's formulation (33) and our formulation (34) are, in general, similar. Here "similar" means that they have the same rate of convergence (in N^{-1} since there is a contrast in ρ) and their relative accuracies depend on the configuration and of the frequency. But a noticeable fact is the following: The accuracy of the formulation (33) decreases of about two orders of magnitude between the lamellar profile (a) and the two other profiles; this is expected since for nonlamellar profiles, one should use the more involved formulation proposed in Ref. 23 instead of the formulation (33). On the

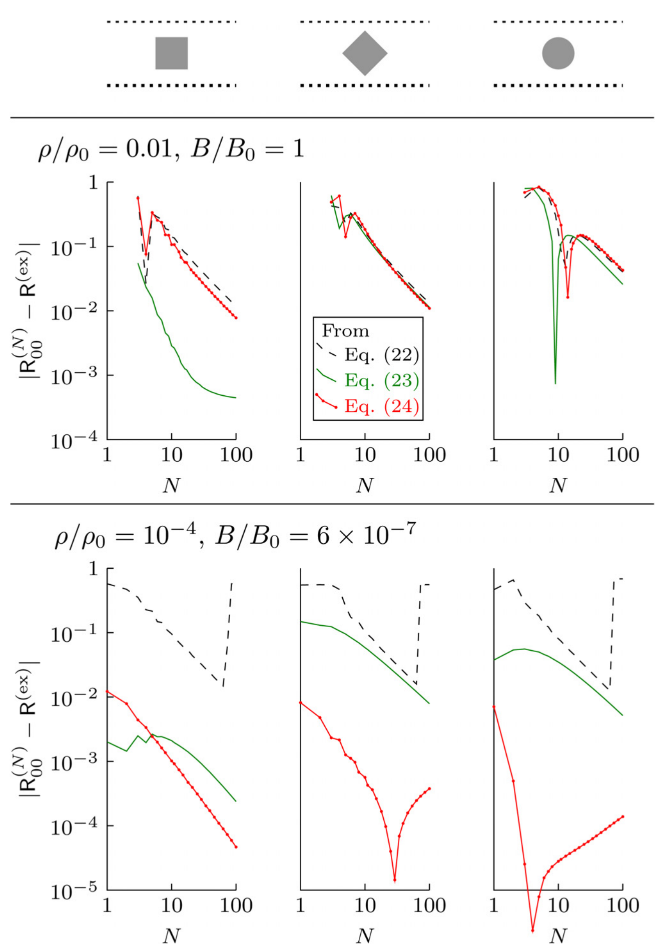

FIG. 5. (Color online) Error $|\mathsf{R}_{00}^{(N)} - \mathsf{R}^{(ex)}|$, from the formulations (32) (dashed lines), (33) (plain), and (34) (plain dotted), for three scatterer geometries. Top: nonmagnetic material, $B/B_0 = 1$ and $\rho/\rho_0 = 0.01$, Bottom: nearly sound hard material, $B/B_0 = 6 \times 10^{-7}$ and $\rho/\rho_0 = 10^{-4}$. Left: square, center: rotated square, right: circular scatterer. Both the square side and the circle diameter are equal to $h/2$.

contrary, the accuracy of our formulation (34) is roughly constant for the three scatterer shapes. A more complete study on the relative accuracy of the coupled-wave methods will be reported elsewhere. Presently, we do not have explanations for the observed differences. However, our weak formulation naturally takes into account the boundary conditions at the scatterer boundaries, which means for instance, that the second-order Eq. (12), equivalent to Eq. (34), accounts for the real shape of the scatterer (for instance, the normal derivative to the scatterer).

IV. ANALYTICAL SOLUTION IN THE WEAK SCATTERING APPROXIMATION

A. Plane wave approximation, generalized Webster equation

Considering the plane wave approximation (PWA), the wave equation deduced from a weak formulation is used to determine analytical solutions that are then compared with the full numerical solution of Eq. (10) using the admittance method. The geometry of Fig. 1 (case A) is considered in this section. From the second-order Eq. (12) at low frequency, $p(x,y) \simeq p_0(x)$ [denoted by $p(x)$ in the following] satisfies the equation

$$(h_\mathrm{w} p')' + k^2 h_\mathrm{w} p = -\frac{\rho}{\rho_0}(h_\mathrm{s} p')' - \frac{B}{B_0} k^2 h_\mathrm{s} p, \tag{35}$$

where $h_\mathrm{s}(x) \equiv b(x) - a(x)$ and $h_\mathrm{w} \equiv h - h_\mathrm{s}$ are the local heights of the part in the waveguide occupied by the scatterer and by the host medium, respectively, and where we have used $C_{00} \simeq h_s/h$ and $D_{00} \simeq 0$. Obviously, the limit $\rho/\rho_0 \to 0$ and $B/B_0 \to 0$ that corresponds to the limit of Neumann boundary condition (thus a waveguide with varying cross section) leads to the usual Webster equation $(h_\mathrm{w} p')' + k^2 (h_\mathrm{w} p) = 0$ with h_w the varying cross section.

Next, two cases are inspected, where analytical predictions are possible. The first case corresponds to the Born approximation already considered in Ref. 24. This is simply done by considering the above equation written as a wave equation with a source term $s(p)$,

$$\begin{cases} p'' + k^2 p = s(p) \\ s(p) = -\dfrac{\rho}{\rho_0}\dfrac{h_\mathrm{s}}{h_\mathrm{w}} p'' - \left(\dfrac{\rho}{\rho_0} - 1\right)\dfrac{h'_\mathrm{s}}{h_\mathrm{w}} p' - \dfrac{B}{B_0} k^2 \dfrac{h_\mathrm{s}}{h_\mathrm{w}} p. \end{cases} \tag{36}$$

The Born solution is obtained by convoluting the one dimensional Green's function with the source term written at leading order $s(p) \simeq s(p^{(\mathrm{inc})})$. In reflection $p = p^{(\mathrm{inc})} + \mathsf{R} e^{-ikx}$ (here, R is a scalar), and R is given by

$$\mathsf{R} = \int \mathrm{d}x' \frac{e^{ikx'}}{2ik} s[p^{(\mathrm{inc})}(x')]. \tag{37}$$

In the case of a local, discontinuous, narrowing, h_w is written

$$h_\mathrm{w}(x) = \begin{cases} h_\mathrm{w} & \text{if } 0 < x < L, \\ (h + h_\mathrm{w})/2 & \text{if } x = 0,\, L, \\ h & \text{otherwise,} \end{cases} \tag{38}$$

and we get $h'_s(x) = (h - h_\mathrm{w})[\delta(x) - \delta(x - L)]$, leading to the reflection coefficient R_E of the expansion

$$\mathsf{R}_\mathrm{E} = \frac{h - h_\mathrm{w}}{h + h_\mathrm{w}}(1 - e^{2ikL}) \left[1 - \frac{\rho}{\rho_0} + \frac{h + h_\mathrm{w}}{4h_\mathrm{w}}\left(\frac{\rho}{\rho_0} - \frac{B}{B_0}\right)\right]. \tag{39}$$

In the case of an homogeneous guide with varying cross section (Neumann boundary condition, obtained for ρ/ρ_0, $B/B_0 \to 0$) is recovered the usual expression

$$\mathsf{R}_\mathrm{E}^{(\mathrm{Neum})} = \frac{h - h_\mathrm{w}}{h + h_\mathrm{w}}(1 - e^{2ikL}). \tag{40}$$

A second case of interest, although somehow artificial, leads to an exact analytical solution. Kumar and Sujith[36] show that the classical Webster equation has an exact solution for $h_\mathrm{w}(x) = A\cos^2(\kappa x)$ [indeed, $P(x) \equiv p(x)\cos(\kappa x)$ satisfies the classical wave equation $P'' + (\kappa^2 + \kappa^2)P = 0$]. In our case, this can be used considering the same contrast in ρ and B. Under this assumption, the classical Webster equation is obtained

$$\begin{cases} (Hp')' + k^2 H p = 0, \\ H \equiv h + \left(\dfrac{\rho}{\rho_0} - 1\right) h_\mathrm{s}, \end{cases} \tag{41}$$

and it is possible to build a smooth variation of h_s such that $h_\mathrm{s} = 0$ for $|x| > L/2$ and such that for $|x| < L/2$ we get $H = A\cos^2(\kappa x)$. This requires $\tan^2(\kappa L/2) = (\rho/\rho_0 - 1)\Delta h/h$, where $\Delta h = h_\mathrm{s}(0)$. The reflection coefficient R_S and the transmission coefficient T_S due to the smooth variations of h_s can now be determined by solving the following system (with the continuity of p and p' at the interfaces $x = \pm L/2$),

$$\begin{cases} p(x \le -L/2) = e^{ikx} + \mathsf{R}_S\, e^{-ikx}, \\ p(|x| \le L/2) = \dfrac{a e^{iKx} + b e^{-iKx}}{\cos \kappa x}, \\ p(x \le -L/2) = \mathsf{T}_S\, e^{ikx}, \end{cases} \tag{42}$$

with $K^2 \equiv k^2 + \kappa^2$ and where the solution $p(|x| \le L/2)$ corresponds to the exact solution of the approximated Webster problem. The reflection coefficient reads as

$$\mathsf{R}_\mathrm{S} = \frac{[\tilde\kappa^2 - \kappa^2]\sin KL + 2K\tilde\kappa\cos KL}{[K^2 + (k + i\tilde\kappa)^2]\sin KL - 2K(\tilde\kappa - ik)\cos KL}, \tag{43}$$

with $\tilde\kappa = \kappa\tan\kappa L/2$ (κ and $\tilde\kappa$ depend on the characteristics of the scatterer only). Results are shown on Fig. 6 in the case of the narrowing and in the case of the smooth cosine form. The expressions obtained appear to be in good agreement with the direct numerics for $kh < 0.8\pi$, afterward resonant phenomena appear. The numerics has been performed solving Eq. (10) with $N = 20$ modes using the admittance method. Note that the reflection extinctions are obtained at different frequencies, given by $kL = n\pi$ for the expansion (R_E), and $\tan(KL)/K = \tan(\kappa L)/\kappa$ for the cosine form (R_S).

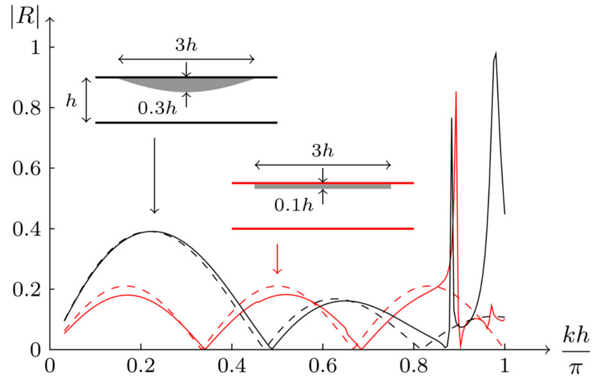

FIG. 6. (Color online) Plane wave reflection coefficient of a waveguide segment with a discontinuous narrowing, and a smooth, sine shaped, narrowing as a function of the nondimensional frequency kh/π with $\rho/\rho_0 = B/B_0 = 3$. Plain lines: numerical solution calculated with $N = 20$ modes, dashed lines: analytical solutions.

B. Periodic grating Wood anomalies

In this paragraph it is shown that the use of the admittance matrix is an efficient tool to get analytical approximated solutions. This is exemplified on the Wood anomaly.

In 1965, Hessel and Oliner[27] explained the main features of the anomalies observed by Wood in 1902.[37] Namely, they consider the system

$$[\mathsf{K} + \mathsf{Y}]\,\mathbf{p} = 2\mathsf{K}\mathbf{p}^{(\mathrm{inc})} \tag{44}$$

equivalent to our Eq. (15) (with $\mathbf{p}^{(\mathrm{r})} = \mathbf{p} - \mathbf{p}^{(\mathrm{inc})}$), and pointed out two families of frequencies, or wavenumbers k, able to produce a rapid variation of the reflection coefficients: (i) the Rayleigh wavenumbers, associated to the branch points $k_n = 0$ for some n value, and (ii) resonance wavenumbers associated to complex poles of p_n in the vicinity of $[\mathsf{K} + \mathsf{Y}]_{nn} = 0$. Below we derive an explicit expression of Y to solve Eq. (44) in the weak scattering approximation, which translates in $\mathsf{Y} = \mathsf{K} + \mathsf{y}$ and $\|\mathsf{y}\| \ll \|\mathsf{K}\|$.

For simplicity, the calculations are performed for a plane wave at normal incidence to the grating with centered symmetrical scatterers, so that the Neumann waveguide configuration can be used. By symmetry, only the even modes are excited. The system in Eq. (44) can be written

$$\begin{bmatrix} 1+\mathsf{z}_{00} & \mathsf{z}_{02} & \cdots & \mathsf{z}_{0N} \\ \mathsf{z}_{20} & 1+\mathsf{z}_{22} & & \vdots \\ \vdots & & \ddots & \\ \mathsf{z}_{N0} & \cdots & & 1+\mathsf{z}_{NN} \end{bmatrix} \begin{bmatrix} p_0 \\ p_2 \\ \vdots \\ p_N \end{bmatrix} = \begin{bmatrix} 1 \\ 0 \\ \vdots \\ 0 \end{bmatrix}, \tag{45}$$

where

$$\mathsf{z}_{nm} = \mathsf{y}_{nm}(0)/2ik_n, \tag{46}$$

for scatterers occupying $[0,\ L]$ (see Fig. 1) and with $\mathsf{y}_{nm}(0) = \mathcal{O}(\epsilon)$ where ϵ measures the small scattering strength. It follows that $\mathsf{R}\mathbf{p}^{(\mathrm{inc})} = -(\mathsf{I} + \mathsf{z})^{-1}\mathsf{z}\mathbf{p}^{(\mathrm{inc})}$, which reduces to, at dominant order,

$$\mathsf{R}_{n0}(k) \simeq -\frac{\mathsf{z}_{n0}}{1 + \sum_j \mathsf{z}_{jj}}. \tag{47}$$

Let us comment the above result. The reflection $\mathsf{R}_{n0} \simeq -z_{n0}$ is in general small. It departs from this simple behavior in two cases. First, near a Rayleigh wavenumber $k_m = 0$: the quantity z_{n0} is still $\mathcal{O}(\epsilon)$ for $n \neq m$ since k_n does not vanish. However, both quantities z_{m0} and $1 + \Sigma\,\mathsf{z}_{jj} \simeq \mathsf{z}_{mm}$ become possibly very large. From Eq. (46), they become of order $\mathcal{O}(\epsilon)/k_m$. Second, at the wavenumber that produces $1 + \mathsf{z}_{mm} = 0$, all the reflection coefficients become of order unity.

To go further, the condition $1 + \mathsf{z}_{mm} = 0$ is inspected. This relation is equivalent to $\mathsf{y}_{mm}(0) = -2ik_m$, Eq. (46). Thus, the corresponding wavenumber $k_m = \mathcal{O}(\epsilon)$ is small. This implies that the second Wood anomaly occurs at a wavenumber close to the Rayleigh wavenumber. Although the predictions in Eq. (47) are not expected to be accurate at these resonances, since we have assumed $\mathsf{z}_{mn} \ll 1$, they are able to capture the rapid variations of R_{n0},

$$\begin{cases} \text{(i)}\ \ k_m = 0, & \mathsf{R}_{n\neq m,0} \simeq \dfrac{-\mathsf{z}_{n0}}{\mathsf{z}_{mm}} \to 0, \\ & \mathsf{R}_{m0} \simeq \dfrac{-\mathsf{z}_{m0}}{\mathsf{z}_{mm}} \to \mathcal{O}(1), \\ \text{(ii)}\ \ 1 + \mathsf{z}_{mm} = 0, & \mathsf{R}_{n0} \simeq -\dfrac{-\mathsf{z}_{n0}}{\sum_{j\neq m} \mathsf{z}_{jj}} \to \mathcal{O}(1). \end{cases} \tag{48}$$

Next, the specific form of z_{n0} and z_{nn} are derived in the case of penetrable scatterers. To do that, the Ricatti equation (49) is linearized (assuming that F and $\mathsf{e} \equiv \mathsf{E} - \mathsf{I}$ are small). Given $\mathsf{A} \equiv -\mathsf{KeK} - \mathsf{F}$, the linearized equation reduces to

$$\mathsf{y}' = -\mathsf{yK} - \mathsf{Ky} - \mathsf{A}. \tag{49}$$

Here, a rectangular scatterer of small size is considered. Note that larger sizes with smaller contrasts could be considered to get weak scattering. The scatterer shape is given by $a(x) = (h - h_s)/2,\ b(x) = (h + h_s)/2\ (h_s \ll h)$, for $x_{\min} = 0 < x < x_{\max} = L$ (Fig. 2). This leads to a piecewise constant matrix A, and the linearized Ricatti equation can be solved analytically starting from the radiation condition $\mathsf{Y}(x_{\max}) = 0$ to get $\mathsf{y}_{nm}(0) = \mathsf{A}_{nm} L \mathcal{S}_{nm}$, with $\mathcal{S}_{nm} \equiv \mathrm{sinc}([k_n + k_m]L/2)e^{i(k_n+k_m)L/2}$ a shape factor. The matrix A_{nm} is calculated using Eqs. (9)–(11) and the quantities z_{nn} and z_{n0} are deduced,

$$\begin{cases} \mathsf{z}_{nn} = \dfrac{(2-\delta_{n0})}{2ik_n}\dfrac{h_s L}{h}\left[k_n^2\left(\dfrac{\rho}{\rho_0} - 1\right) + k^2\left(\dfrac{B}{B_0} - 1\right)\right]\mathcal{S}_{nn}, \\ \mathsf{z}_{n0} = \dfrac{\sqrt{(2-\delta_{n0})}}{2ik_n}\dfrac{h_s L}{h}k\left[k_n\left(\dfrac{\rho}{\rho_0} - 1\right) + k\left(\dfrac{B}{B_0} - 1\right)\right]\mathcal{S}_{n0}. \end{cases} \tag{50}$$

Some refinements with respect to our general comments above can be done. From Eq. (50), it can be seen that the Rayleigh anomaly only occurs if a contrast in B exists.

Indeed, if not the case, $z_{nn} \propto k_n$ and $z_{0n} \propto 1$ instead of being proportional to $1/k_n$ as expected from the expression in Eq. (46). To the opposite, for $B \neq B_0$, both z_{nn} and z_{n0} are proportional to $1/k_n$. Next, the condition for the second anomaly implies $z_{nn} = -1$. Inspecting Eq. (50) leads to the following conclusions: the second Wood anomaly occurs if k_n is purely imaginary, thus below the Rayleigh anomaly at $k_n = 0$. This will produce a max−min Fano resonance type.[38] This condition can be easily obtained, e.g., for no contrast in ρ and for $B > B_0$, and the distance between the max and the min is measured by the small $y_{nn}/2$.

To summarize, for small penetrable scatterers,

(1) for a contrast in ρ only, no anomalies are expected,
(2) for a contrast in B only: if $B < B_0$, only the Rayleigh anomaly is expected, and for $B > B_0$, a resonant anomaly (with maximum reflection value) preceding a Rayleigh anomaly is expected. This corresponds to a Fano type resonance.

We have considered an incident plane wave at normal incidence to an array of square scatterers with $h_s = L = h/10$. The frequency range is such that $kh \in [0, 4\pi]$, thus passing through two cutoff frequencies of even modes at $kh = 2\pi$ and 4π. We have checked that no anomalies are observed for no contrast in ρ (results are not reported). The results for a contrast in B are shown on Fig. 7. The comparison of our analytical expression (47) with direct numerics shows a good agreement both for $B/B_0 < 1$ (only the Rayleigh Wood anomaly is observed) and for $B/B_0 > 1$ where the two anomalies occur, leading to a Fano shape behavior.

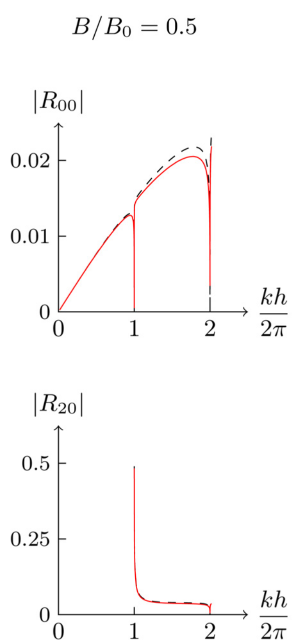

FIG. 7. (Color online) Reflection coefficients R_{00} and R_{20} as a function of the nondimensional frequency $kh/2\pi$ for a plane wave at normal incidence to a grating made of square penetrable scatterers of side $h_s = h/10$, mass density $\rho_0 = \rho$, and a bulk modulus B_0 such that $B/B_0 = 0.5$ (left), $B/B_0 = 2$ (right). Plain lines: numerical results, dashed lines: analytical.

V. CONCLUSION

We have presented a multimodal method based on the use of the admittance matrix to describe the acoustic propagation through arbitrary shaped penetrable scatterers, located in a rigid waveguide or forming a periodic array. Our coupled wave equations are based on a weak formulation. Together with the local admittance formulation, it leads to an efficient and easily implementable numerical method, well suited to describe continuously variable shape of scatterers, beyond the usual staircase approximation. Besides, the reciprocity and energy conservation of the initial problem are preserved in our numerical scheme. Works are in progress to better understand the influences of the projection method and of the truncation rules as discussed in Refs. 22 and 23 on the convergence and accuracy of the numerical schemes in multimodal methods.

The formulation presented in this paper allowed to develop analytical calculations in limiting cases. This has been illustrated in two examples of interest: The generalization of the Webster equation, which describe the acoustic propagation in the low frequency limit, and the derivation of the reflection coefficients by a periodic array of small scatterers, leading to a quantitative prediction of the Wood anomalies. The use of the Riccati differential equation for the impedance matrix is a key point of our resolution in this latter case, and certainly, this kind of approach may be used in a large class of scattering problems.

ACKNOWLEDGMENTS

We acknowledge Vincent Pagneux for fruitful discussions. This work has been supported by the Agence Nationale de la Recherche, through the grant ANR ProCoMedia, project ANR-10-INTB-0914.

[1]P. M. A. Sloot and C. G. Figdor, "Elastic light scattering from nucleated blood cells: rapid numerical analysis," Appl. Opt. **25**, 3559–3565 (1986).
[2]M. Chekroun, L. Le Marrec, B. Lombard, and J. Piraux, "Time-domain numerical simulations of multiple scattering to extract elastic effective wavenumbers," Waves Random Complex Media **22**, 398–422 (2012).
[3]I. D. Chremmos and N. K. Uzunoglu, "Analysis of scattering by a linear chain of spherical inclusions in an optical fiber," J. Opt. Soc. Am. A **23**, 3054–3062 (2006).
[4]C. M. Linton and I. Thompson, "Resonant effects in scattering by periodic arrays," Wave Motion **44**, 165–175 (2007).
[5]J. O. Vasseur, B. Morvan, A. Tinel, N. Swinteck, A.-C. Hladky-Hennion, and P. A. Deymier, "Experimental evidence of zero-angle refraction and acoustic wave-phase control in a two-dimensional solid/solid phononic crystal," Phys. Rev. B **86**, 134305 (2012).
[6]M. Farhat, S. Guenneau, S. Enoch, G. Tayeb, A. B. Movchan, and N. V. Movchan, "Analytical and numerical analysis of lensing effect for linear surface water waves through a square array of nearly touching rigid square cylinders," Phys. Rev. E **77**, 046308 (2008).
[7]Y. Pennec, B. Djafari-Rouhani, H. Larabi, J. O. Vasseur, and A.-C. Hladky-Hennion, "Low-frequency gaps in a phononic crystal constituted of cylindrical dots deposited on a thin homogeneous plate," Phys. Rev. B **78**, 104105 (2008).
[8]P. J. Cobelli, V. Pagneux, A. Maurel, and P. Petitjeans, "Experimental study on water-wave trapped modes," J. Fluid Mech. **666**, 445–476 (2011).
[9]M. A. Peter, M. H. Meylan, and C. M. Linton, "Water-wave scattering by a periodic array of arbitrary bodies," J. Fluid Mech. **548**, 237–256 (2006).

[10]K. S. Chiang, "Review of numerical and approximate methods for the modal analysis of general optical dielectric waveguides," Opt. Quantum Electron. **26**, 113–134 (1994).
[11]C. Vassallo, "1993−1995 optical mode solvers," Opt. Quantum Electron. **29**, 95–114 (1997).
[12]V. Pagneux, N. Amir, and J. Kergomard, "A study of wave propagation in varying cross section waveguides by modal decomposition—Part 1: Theory and validation," J. Acoust. Soc. Am. **100**, 2034–2048 (1996).
[13]R. Caussé, J. Kergomard, and X. Lurton, "Input impedance of brass musical instruments—Comparison between experiment and numerical models," J. Acoust. Soc. Am. **75**, 241–254 (1984).
[14]N. Amir, V. Pagneux, and J. Kergomard, "A study of wave propagation in varying cross section waveguides by modal decomposition—Part II: Results," J. Acoust. Soc. Am. **101**, 2504–2517 (1997).
[15]S. Félix, J.-P. Dalmont, and C. J. Nederveen, "Effect of bending portions of the air column on the acoustical resonances of a wind instrument," J. Acoust. Soc. Am. **131**, 4164–4172 (2012).
[16]S. Félix and V. Pagneux, "Sound propagation in rigid bends: A multimodal approach," J. Acoust. Soc. Am. **110**, 1329–1337 (2001).
[17]S. Félix and V. Pagneux, "Multimodal analysis of acoustic propagation in three dimensional bends," Wave Motion **36**, 157–168 (2002).
[18]V. Pagneux and A. Maurel, "Lamb wave propagation in inhomogeneous elastic waveguides," Proc. R. Soc. London Ser. A **458**, 1913 (2002).
[19]L. Li, "Formulation and comparison of two recursive matrix algorithms for modeling layered diffraction gratings," J. Opt. Soc. Am. A **13**, 1024–1035 (1996).
[20]B. Gralak, S. Enoch, and G. Tayeb, "From scattering or impedance matrices to Bloch modes of photonic crystals," J. Opt. Soc. Am. A **19**, 1547–1554 (2002).
[21]M. G. Moharam and T. K. Gaylord, "Rigorous coupled-wave analysis of planar-grating diffraction," J. Opt. Soc. Am. **71**, 811–818 (1981).
[22]L. Li, "Use of Fourier series in the analysis of discontinuous periodic structures," J. Opt. Soc. Am. A **13**, 1870–1876 (1996).
[23]E. Popov and M. Nevière, "Grating theory: new equations in Fourier space leading to fast converging results for TM polarization," J. Opt. Soc. Am. **17**, 1773–1784 (2000).
[24]A. Maurel and J.-F. Mercier, "Propagation of guided waves through weak penetrable scatterers," J. Acoust. Soc. Am. **131**, 1874–1889 (2012) [Erratum: J. Acoust. Soc. Am. **132**, 1230 (2012)].
[25]A. G. Webster, "Acoustical impedance, and the theory of horns and of the phonograph," Proc. Natl. Acad. Sci. U.S.A. **5**, 275–282 (1919).
[26]S. W. Rienstra, "Webster's horn equation revisited," SIAM J. Appl. Math. **65**, 1981–2004 (2005).
[27]A. Hessel and A. A. Oliner, "A new theory of Wood's anomalies on optical gratings," Appl. Opt. **4**, 1275–1297 (1965).
[28]V. Pagneux, "Multimodal admittance method in waveguides and singularity behavior at high frequency," J. Comput. Appl. Math. **234**, 1834–1841 (2010).
[29]V. Pagneux and A. Maurel, "Lamb wave propagation in elastic waveguides with variable thickness," Proc. R. Soc. A **462**, 1315–1339 (2006).
[30]S. Félix and V. Pagneux, "Ray-wave correspondence in bent waveguides," Wave Motion **41**, 339–355 (2005).
[31]A. David, H. Benisty, and C. Weisbuch, "Fast factorization rule and plane-wave expansion method for two-dimensional photonic crystals with arbitrary hole-shape," Phys. Rev. B **73**, 075107 (2006).
[32]V. Pagneux and A. Maurel, "Scattering matrix properties with evanescent modes for waveguides in fluids and solids," J. Acoust. Soc. Am. **116**, 1913–1920 (2004).
[33]A. Barnett and L. Greengard, "A new integral representation for quasi-periodic scattering problems in two dimensions," BIT Numer. Math. **51**, 67–90 (2011).
[34]D. Martin, *Melina Version 2.5* (2011), http://anum-maths.univ-rennes1.fr/-melina/danielmartin/melina/ (Last viewed 6/6/13).
[35]J.-F. Mercier and A. Maurel, "Acoustic propagation in non uniform waveguides: revisiting Webster equation using evanescent boundary modes," Proc. R. Soc. A **469**, 20130186 (2013).
[36]B. M. Kumar and R. I. Sujith, "Exact solutions for the longitudinal vibration of nonuniform rods," J. Sound Vib. **207**, 721–729 (1997).
[37]R. W. Wood, "On a remarkable case of uneven distribution of light in a diffraction grating spectrum," Philos. Mag. **4**, 396–402 (1902).
[38]U. Fano, "Effects of configuration interaction on intensities and phase shifts," Phys. Rev. **124**, 1866–1878 (1961).